LIN7 regulates the filopodia and neurite promoting activity of IRSp53

[1]*Arianna Crespi, [1]*Ilaria Ferrari, [1]Paola Lonati, [2]Andrea Disanza, [1,4] Diego Fornasari, [2,3]Giorgio Scita, [1]Valeria Padovano, and [1,4,5] Grazia Pietrini.

[1] Department of Medical Biotechnology and Translational Medicine, Università degli Studi di Milano, Milan, Italy

[2] IFOM, FIRC Institute of Molecular Oncology Foundation at IFOM-IEO Campus, Milan, Italy

[3] Dipartimento di Medicina, Chirurgia e Odontoiatria, Università degli Studi di Milano, Milan, Italy

[4] CNR-Institute of Neuroscience, Milan, Italy

[5] Corresponding author: Grazia PIETRINI,
Department of Medical Biotechnology
and Translational Medicine
Via Vanvitelli 32, 20129 Milano, Italy
Phone: +39 02 50317094
FAX: +39 02 7490574
E-mail: grazia.pietrini@unimi.it

*These authors equally contributed to this project

Running title: LIN7 regulation of IRSp53

JCS online publication date 5 July 2012

SUMMARY

The insulin receptor substrate protein of 53 kDa (IRSp53) is critically involved in the formation of filopodia and neurites through mechanisms that have only in part been clarified. Here, we investigated the role of the small scaffold protein LIN7, an interactor of IRSp53. We found that formation of actin-filled protrusions in neuronal NSC34 cells and neurites in neuroblastoma N2A depends on motifs mediating the LIN7:IRSp53 association, as both the coexpression of LIN7 with IRSp53 or the expression of the L27-IRSp53 chimera (a fusion protein between IRSp53 and the LIN7L27 domain for plasma membrane protein complexes association) prevented actin-deficient protrusions induced by overexpressed IRSp53, and enhanced the formation of actin-filled protrusions. The regulatory role of LIN7 in IRSp53-mediated extension of filopodia was demonstrated by live-cell imaging experiments in neuronal N2A cells. Moreover, LIN7 silencing prevented the extension of filopodia and neurites, induced by ectopic expression of IRSp53 or serum starvation, respectively in undifferentiated and differentiated N2A cells. The expression of full length IRSp53 or the LIN7ΔPDZ mutant lacking the domain for association with IRSp53 was unable to restore neuritogenesis in LIN7 silenced cells. Conversely, defective neuritogenesis could be rescued by the expression of RNAi-resistant full length LIN7 or chimeric L27-IRSp53. Finally, LIN7 silencing prevented the recruitment of IRSp53 in Triton X-100 insoluble complexes, otherwise occurring in differentiated cells. Collectively these data indicate that LIN7 is a novel regulator of IRSp53, and that their association is required to promote the formation of actin-dependent filopodia and neurites.

INTRODUCTION

To explore the environment and make contacts with other cells and/or the substratum, several cell types extend rod-like surface projections filled with bundles of parallel actin filaments (F-actin), called filopodia. In neuronal cells, filopodia emerging from dendrites and axons are essential for synapse and neurite initiation (Ziv and Smith, 1996; Dent et al., 2007), while those emanating from growth cones are involved in their directional motility (Lowery and Van Vactor, 2009).

The molecular details of the initiation and maintenance of these protrusions have been the subject of intense investigations. A number of crucial molecular players, mostly controlling the dynamic and architectural organisation of actin filaments at the bases of filopodia formation have been identified. For example, a pivotal role is played by a filopodial tip multiprotein complex located at the interface between the growing ends of actin filaments and the plasma membrane (Faix and Rottner, 2006). The tip complex contains a variety of actin-associated proteins, which possess different functional and biochemical roles, including binding and/or sequestering of actin monomers, nucleation of actin filaments, capping or anti-capping of barbed ends, severing, bundling and anchoring of actin filaments (Faix and Rottner, 2006).

A key molecule of the tip complex is the insulin receptor substrate protein of 53 kDa (IRSp53) (Nakagawa et al., 2003). At the signaling levels, IRSp53 likely acts as an effector protein that physically links activated Rho-GTPases, such as Cdc42 and Rac (Krugmann et al., 2001), with a variety of actin regulatory proteins (Ahmed et al., 2010), further restricting their cellular localisation to the plasma membrane. IRSp53 was identified as the founding member of a family of proteins featuring the presence of the so-called IRSp53 and missing-in-metastasis (MIM) homology domain, IMD (Lee et al., 2002). This domain belongs to the larger family of the Bin–Amphiphysin–Rvs167 (BAR) domain that binds to phospholipid-rich lipid bilayers of different curvatures. Most BAR domains display a concave, banana-shaped structure, which is critical to promote positive membrane curvature leading to invagination. IRSp53 inverted BAR domain (I-BAR) folds, instead, into a straight cigar-shaped dimer, with a distribution on its convex side of positively-charged residues that contact negatively-charged membranes, thus promoting negative membrane curvature typical of filopodia protrusions (Scita et al., 2008; Zhao et al., 2011). In keeping with this latter notion, the ectopic expression of the I-BAR domain alone is sufficient to induce filopodia-like protrusions that, however, exhibit a low content of F-actin (Mattila et al., 2007; Yang et al., 2009). The efficient formation of actin-filled protrusions requires Rho GTPases activation of IRSp53 at the plasma membrane (Krugmann et al., 2001). At this location, IRSp53 may initiate membrane deformation by recruiting a variety of actin regulators, including Mena (Ena/VASP) family proteins, N-WASP, mDia, and Eps8 (Scita et al., 2008), through its SH3 domain. Thus, IRSp53

may couple membrane protrusions and F-actin for filopodia extension from the cell periphery (Ahmed et al., 2010).

During the last years, a role for IRSp53-mediated filopodia in neuritogenesis has also emerged: neurites have been shown to form from dilation of a single stable filopodium (Dent et al., 2007), the ectopic expression of IRSp53 induces neurite formation (Miki and Takenawa, 2002), whereas IRSp53 silencing reduces neurite outgrowth (Goh et al., 2011a). The precise molecular mechanisms of IRSp53-mediated formation of filopodia and neurites, however, remain ill-defined.

Among the three isoforms of IRSp53 (L, S, and IRS-58) identified in rodents, the long (L) and short (S) isoforms are predominantly expressed in neurons (Okamura-Oho et al., 2001; Miyahara et al., 2003). The shorter IRSp53 (also known as BAIAP2α, brain-specific angiogenesis inhibitor-1 associated protein 2α) is the only isoform containing a PDZ (PSD-95/Discs large/Zona occludens-1)-target motif at its C-terminal end for interaction with proteins containing class 1 PDZ domains, including LIN7/MALS (mammalian LIN seven) proteins (Hori et al., 2003), the PSD-95 and chapsyn-110/PSD-93 members of the PSD-95 (postsynaptic density 95) family (Choi et al., 2005) and the neuronal channel-interacting PDZ protein CIPP (Barilari and Dente, 2010).

The physiological role of the various PDZ proteins in IRSp53 function is still unclear, but data indicating their function in the engagement of IRSp53 with macromolecular junctional complexes in polarised epithelial MDCK cells (Massari et al., 2009), and with post-synaptic density protein complexes in neurons have been provided (Choi et al., 2005; Barilari and Dente, 2010). However, PSD-95 family proteins are involved in late stages of neuronal differentiation that are accompanied by the stabilisation and maturation of filopodia to generate dendritic spines, whereas proteins, like LIN7, localising to both pre- and post-synaptic sites (Jo et al., 1999; Perego et al., 2000; Olsen et al., 2005) may control the early steps of axonal and dendritic filopodia formation during synaptogenesis.

LIN7 is a small scaffold protein possessing only a single L27 domain, necessary for membrane recruitment, and a single PDZ1 domain mediating protein-protein interactions, including the one with IRSp53. The absence of either the L27 or PDZ domains causes mislocalisation of LIN7 as well as IRSp53 in a polarised epithelial cell line (Massari et al., 2009). In particular, the L27 domain of LIN7 is known to mediate heterodimerisation with L27 domain-containing membrane-associated guanylate kinase (MAGUK) proteins, including calcium/calmodulin-dependent serine protein kinase (CASK), protein associated with LIN7 (Pals), synapse-associated protein 97 (SAP97) and isoforms of PSD-95 and PSD-93 (Chetkovich et al., 2002; Feng et al., 2004; Funke et al., 2005), which form the core of protein complexes that mediate synaptic development, plasticity, and functionality (Zheng et al., 2011). In vertebrates, there are three genes,

LIN7-A-B-C also named MALS/Veli-1-2 -3, and alterations in these genes cause renal defects and synaptic dysfunctions (Olsen et al., 2007), and mice harbouring null mutations of all the three LIN7 isoforms die perinatally with respiratory problems and impaired synaptic transmission (Olsen et al., 2005). Moreover, polymorphisms and altered expression of LIN7 have been recently associated with human psychiatric conditions such as attention-deficit/hyperactivity disorder (ADHD) and neurodegenerative diseases (Lanktree et al., 2008; Zucker et al., 2010; Shinawi et al., 2011). Interestingly, certain IRSp53 alleles in humans have also been linked to ADHD (Ribases et al., 2009).

Here we hypothesised that LIN7 is a possible partner of IRSp53 in the early steps of formation of filopodia and neurites; using a combination of structure-function studies with different mutants of either LIN7 or IRSp53 together with RNAi-based depletion in neuronal cell lines, we investigated the functional and molecular role of this protein partnership in filopodia formation and in neuritogenesis. Our morphological and biochemical data indicate a positive regulatory role for LIN7 in the formation of IRSp53-mediated actin-filled filopodia and neurites, and provide further evidence that neuritogenesis depends on actin-stabilised filopodia.

RESULTS

The localisation of LIN7 and IRSp53 in filopodia tips depends on the L27 domain of LIN7 and the PDZ target motif of IRSp53

To gain initial clue as to a role of the LIN7:IRSp53 complex in filopodia, we ectopically expressed various combinations of epitope-tagged, wild type and mutant proteins (Fig. 1A) in NSC34 cells. This motoneuron-like cell line was chosen as model because it exhibits endogenous filopodia-like protrusions (width of ~1 μm and length of ~5-10 μm) containing actin filaments along their entire length. Both myc-IRSp53 and GFP-LIN7, expressed alone or in combination, localised along the entire shafts and often appeared enriched on their tips. Protrusions with club-shaped tips similar to those shown in figure 1B have been previously described in cells expressing constitutively active human formin mDia2 (Yang et al., 2007; Block et al., 2008), suggesting that overexpression of the constructs may activate formins (see also the Discussion in relation to this point). The IRSp53Δ5 construct lacking the association motif for the PDZ domain of LIN7 maintained the localisation along the shafts, but completely lost the tip enrichment (Fig. 1B, see plot profiles of the representative filopodia), suggesting that an interaction with PDZ-containing proteins endogenously expressed by these cells, such as LIN7, may be crucial for proper targeting of IRSp53. To strengthen this notion, we used a chimeric construct in which the LIN7-binding-deficient IRSp53Δ5 mutant was targeted to the plasma membrane by adding the L27 domain of LIN7 to its N-terminus (L27-IRSp53Δ5 chimera) (Massari et al., 2009). The L27 domain was sufficient to fully rescue tip localisation of IRSp53Δ5 (compare the plot profile of L27-IRSp53Δ5 chimera in panel C with that of IRSp53Δ5 in panel B). The importance of the L27 domain of LIN7 was further supported by the finding that a LIN7 mutant deleted of the L27 domain (LIN7ΔL27) was excluded from protrusions, and caused the sequestration of the coexpressed IRSp53 in the cytoplasm (Fig. 1C).

The localisation data above described for overexpressed constructs were not verified with endogenous LIN7 and IRSp53, because both proteins were under the level of detection using their specific antibody. However, overexpressed LIN7 and IRSp53 colocalise in protrusions and most prominently at their tips, and these tip enrichments were abolished when interaction between the two proteins was prevented (see a summary of localisation data in panel D), hence suggesting a role for the LIN7:IRSp53 complex in the extension of membrane protrusions.

LIN7 regulates the protrusion promoting activity of IRSp53.

It is well established that the expression of full length IRSp53 as well as of its isolated I-BAR domain is sufficient to induce filopodia-like protrusions in a variety of cell lines. Notably, however,

these protrusions, particularly when induced by the I-BAR domain of IRSp53, differ from canonical filopodia since they generally display a lower content of organised F-actin. In addition, the transfected proteins are uniformly distributed along the entire shaft, instead of being enriched at the tips of the protrusions (Faix and Rottner, 2006; Mattila et al., 2007; Yang et al., 2009). We obtained similar results in NSC34 cells. In these cells, the expression of IRSp53 or IRSp53Δ5 induced a large number of protrusions that appeared floppy and branched, and frequently devoid of F-actin, which could, instead, be detected mainly at the bases of these structures (Fig. 2A-B). Notably, however, a "normal" morphology and structural organisation was restored by the concomitant expression of LIN7 and IRSp53, but not with IRSp53Δ5 (see Fig. 1B for protrusion magnification). Aberrant, actin-deficient protrusions were also virtually absent in cells expressing the chimeric protein L27-IRSp53Δ5 (Fig. 2C and see Fig. 1C for protrusion magnification). Since comparable levels of expression of the IRSp53 constructs were measured by Western blot analysis (see Fig. S1 in supplementary material), these data suggest that LIN7 coexpression is necessary and sufficient to prevent the aberrant protrusions induced by overexpressed IRSp53. It is of note that the mean total number of protrusions (actin-filled + actin deficient) significantly increased under all conditions of transfection tested (Fig. 2D), albeit it was less pronounced in cells coexpressing LIN7 with IRSp53 or the L27-IRSp53Δ5 chimera alone, which remarkably displayed only actin-filled protrusions. These results therefore reinforce a critical role of LIN7 in promoting IRSp53-mediated, F-actin-positive protrusions.

The effect of LIN7:IRSp53 association on F-actin was also analysed by measuring the ratio of F-actin/monomeric G-actin (Fig. 2E). This assay is based on the differential extractability of F- and G-actin from cells by non-ionic detergent (Blikstad and Carlsson, 1982). We found unaltered F- to G-actin ratio in cells expressing IRSp53Δ5, whereas it was significantly increased in cells expressing the L27-IRSp53Δ5 chimera, further supporting that LIN7-mediated plasma membrane recruitment of IRSp53 is necessary for the stabilisation of actin in protrusions induced by the ectopic expression of IRSp53.

Effect of IRSp53 and L27-IRSp53 on filopodia dynamic in live-cell imaging

Based on morphological criteria, the protrusions of 5-10 μm length and width of ~1 μm containing actin for their entire length described in NSC34 cells could be considered filopodia (Yang and Svitkina, 2011). However, filopodia are defined as highly dynamic protrusions undergoing rapid cycles of extension and resorption, we therefore analysed the role of LIN7 in filopodia extension by live-cell imaging experiments. These experiments were performed in neuroblastoma N2A cells because of their high efficiency of transfection and tolerance to the environmental and illumination

conditions (laser light) during time-lapse recording. Moreover, N2A cells behave like proliferating, undifferentiated neuroblasts when grown in the presence of serum, while extend filopodia and neurites upon serum deprivation (Wu et al., 1998).

We compared filopodia induced by 16 h serum starvation in cells expressing GFP-tagged IRSp53 or L27-IRSp53 in reconstitution experiments for length and lifetime. In these experiments, the cells were cotransfected with RFP-pLifeAct to identify F-actin-filled filopodia, and cells transfected with GFP fused to a plasma membrane localisation signal (mGFP) were used as control.

The extent of protrusions induced by IRSp53 or L27-IRSp53 expression in differentiated N2A cells were equivalent to those promoted in NSC34 cells, as total protrusions were respectively 1.72-fold (± 0.03) and 1.4-fold (± 0.16) higher than control. Filopodia were positive for LifeAct and the IRSp53 and LIN7 along their lengths (Fig. 3A-C), and their average length (3.44 μm ± 0.36) did not differ significantly from control. The lifetime of filopodia protruding or retracting was significantly decreased from 170 s in the control to 110 s in both IRSp53 and L27-IRsp53 filopodia (examples in A-C, quantification in D, and see Movies 1-3 in supplementary material). However, the time-lapse analysis indicated a 2-fold increase in static linear protrusions in IRSp53 transfected cells compared to control (Fig. 3E). Even the abnormal, branched and F-actin-poor protrusions induced by overexpressed IRSp53 were static during the 5 min examined (Fig. 3G, and see Movie 4 in supplementary material). In sharp contrast, static protrusions were drastically reduced in cells expressing the L27-IRSp53 chimera (Fig. 3E), and almost all the protrusions induced by the chimera were dynamic and thus identified as filopodia. In line with these findings, the total number of filopodia protruding or retracting from 100 μm plasma membrane within 5 min doubled the control in L27-IRSp53 expressing cells, whereas it did not differ significantly in IRSp53 expressing cells (Fig. 3F).

Since the level of expression of the constructs was comparable (see Fig. S2 in supplementary material), these data confirm the results obtained in NSC34 cells concerning the LIN7 control of altered protrusions induced by IRSp53 overexpression and robustly indicate IRSp53 requirement of LIN7 to promote filopodia.

LIN7 is required for IRSp53-induced differentiation of neuronal N2A cells

To further demonstrate the role of LIN7 in filopodia, LIN7 was silenced in N2A cells. Since actin bundling and filopodia formation are critical early steps in neurite formation (Dent et al., 2007), neuritogenesis was analysed in LIN7 silenced N2A cells.

Three different LIN7A, B, C isoforms are frequently ubiquitously expressed: LIN7A is larger with a predicted molecular weight of 29 kDa. LIN7B and C are, instead, smaller and

predicted to have a similar 22 kDa molecular weight. We used a pan-LIN7 antibody (which does not distinguish among the three LIN7 isoforms) to asses which isoforms were expressed in N2A cells by immunoblotting. As shown in Fig. 4A, we could only detect a single 22 kDa band, possibly corresponding to LIN7B and C. The pan-IRSp53 antibody predominantly recognised a doublet (~75% of the total bands) migrating at the expected 50-53 kDa molecular weight for IRSp53-S, with the band of lower mobility probably corresponding to phosphorylated IRSp53-S (Cohen et al., 2011), and a 70 kDa band corresponding to mobility of the IRSp53-L isoform (Okamura-Oho et al., 2001; Miyahara et al., 2003). The doublet was immunoprecipitated by the LIN7 antibody but not by the preimmune serum (bands 1, 2 in the IP). However, bands with molecular weight corresponding to IRSp53-S dimers and tetramers (bands 4-5 in the IP) and, surprisingly, also the band of ~70 kDa was selectively detected in LIN7 immunocomplexes (Fig 4A). All the unexpected bands might be artefacts due to oligomerisation with IRSp53-S occurring in the immunoprecipitation condition.

The 22 kDa band was greatly reduced in N2A cells silenced for LIN7C (Fig. 4B), and the reduction level correlated with the transfection efficiency in this cell system, thus suggesting that LIN7C is the main, if not exclusive, isoform in N2A cells. The LIN7C silencing did not affect the expression of all the IRSp53 endogenous isoforms, but completely prevented the extension of protrusions, recognised as filopodia and neurites on the basis of their length and size, induced by 48 h serum starvation or promoted by IRSp53 overexpression in undifferentiated N2A cells (Fig. 4C and quantification in E). Similar results were obtained with shRNA 2 (see Fig. S3 in supplementary material). The requirement of LIN7 for IRSp53-mediated protrusions appears to be specific, as silencing of LIN7C did not prevent neuritogenesis and filopodia formation induced by mDia1 or mDia2 (Fig. 4D, quantification in E), members of the formin family of proteins that induce filopodia and neurite extension by promoting the nucleation and linear elongation of actin (Faix and Grosse, 2006).

Differentiation of N2A cells requires the L27 and PDZ domains of LIN7.

We further analysed the role of LIN7 in IRSp53-mediated neurite outgrowth and the requirement of the LIN7 domains. To this end, N2A cells were transfected (green signal) with the empty vector (pSUPER) or with cDNA encoding shRNA LIN7C, and 24 h after transfection the cells were cultured in serum-free medium for 48 h to induce differentiation (Fig. 5).

Analysis of phase contrast images (Fig. 5A), and their corresponding quantifications (Fig. 5B), indicate highly significant reduction of neurites induced by serum-starvation in LIN7C silenced cells, confirming the essential function of the LIN7C isoform in neurite extension. The expression of IRSp53 in LIN7C-interferred cells did not restore neuritogenesis, which was, instead,

fully rescued by the expression of the RNA silencing resistant LIN7A isoform. Notably, neuritogenesis was not re-established by the expression of the LIN7 variant lacking the PDZ domain, but it was fully restored by the L27-IRSp53 chimera. Since the levels of expression of the constructs were comparable (see Fig. S4 in supplementary material), these data further demonstrate the requirement of both domains of LIN7 for IRSp53-mediated neuritogenesis.

LIN7 is required to relocate IRSp53 in Triton X-100 insoluble complexes in differentiated N2A cells

If formation of actin-filled protrusions (neurites) during N2A differentiation depends on LIN7 recruitment of IRSp53 to plasma membrane sites, we might expect an increased amount of the latter protein to remain associated with fractions rich in plasma membranes and cytoskeletal elements. Insolubility of a protein to non-ionic detergent is largely dependent on the strength of its association with actin cytoskeleton (Gilbert and Fulton, 1985), we therefore investigated the Triton X-100 solubility of LIN7 and IRSp53 in control and silenced N2A cells (Fig. 6).

Undifferentiated (+FBS) or serum-free medium differentiated (-FBS) N2A cells were lysed in 0.5% Triton X-100 for 10 min at 0°C, and equal volumes of soluble (S) or insoluble (I) fractions were analysed by immunoblotting. The amount of LIN7 and IRSp53 recovered in the Triton X-100 insoluble cytoskeletal-associated fraction increased in differentiated cells, reaching ~60% after 48 h in serum free medium (Fig. 6A). This finding suggests that under conditions of neurite outgrowth there is an increased association of LIN7 and IRSp53 with the F-actin cytoskeleton.

To demonstrate that IRSp53 detergent insolubility depends on LIN7, we characterised three independent N2A clones (2, 5 and 9) stably silenced for LIN7C with shRNA 1 (Fig. 6B). It is of note that the total level of downregulation of IRSp53 was directly proportional to that of LIN7, suggesting that LIN7 protects IRSp53 from degradation. More importantly, a nearly complete absence of neurites (Fig. 6C) and of IRSp53 redistribution in Triton X-100 insoluble fractions (Fig. 6D) was found in silenced cell lines even after 48 h serum-starvation. The defective neuritogenesis observed in these cells coincided with that obtained in transiently silenced cells, where the expression of IRSp53 was unchanged (see Fig. 4B and Fig. S3 in supplementary material), further corroborating the requirement of the LIN7:IRSp53 complex for neuritogenesis.

DISCUSSION

By coupling membrane deformation to actin filament polymerisation, IRSp53 has emerged as one of the key proteins in promoting plasma membrane protrusions (filopodia) considered to be precursors of neurites and polarised structures such as synapses (Ziv and Smith, 1996; Dent et al., 2007). We have previously shown that LIN7 regulates epithelial polarity through its binding and recruitment of IRSp53 to tight junctional plasma membrane domains (Massari et al., 2009), and here, we have tested whether LIN7 regulates the formation of IRSp53-dependent filopodia and neurites.

Our findings indicate that LIN7 plays a positive regulatory role on the filopodia and neurite promoting activity of IRSp53, and that this regulation depends on both protein-protein association domains of LIN7: the PDZ domain for binding to the last C-terminal residues of IRSp53, and the L27 domain for association with plasma membrane protein complexes.

We found that full length LIN7 regulates IRSp53 activity by preventing the formation of actin-deficient abnormal protrusions and by sustaining the extension of F-actin-rich protrusions in NSC34 cells. These findings were confirmed by live-cell imaging experiments in differentiated N2A cells, collectively indicating that static protrusions induced by the overexpression of IRSp53 were abolished in cells overexpressing the L27-IRSp53 chimera, and that virtually all the protrusions in cells overexpressing the L27-IRSp53 chimera were dynamic and thus bona fide identified as filopodia. Moreover, downregulation of LIN7C by shRNA definitively demonstrate the strict requirement of LIN7C isoform in the formation of filopodia and neurites induced by IRSp53, as overexpression of IRSp53 completely failed to induce any protrusions in N2A silenced for LIN7.

LIN7 association with IRSp53 rather than its simple presence was required to control IRSp53 activity, and this is clearly indicated by the fact that LIN7 is not able to prevent the formation of actin-deficient protrusions induced by the expression of the IRSp53Δ5 mutant lacking the interaction motif for LIN7. The additional finding that protrusions unstained or poorly labelled by phalloidin, and thus floppy, are formed in cells expressing either unbalanced levels of IRSp53 and LIN7 or the IRSp53Δ5 mutant, further suggests that the two proteins must operate as a tightly regulated complex for the proper formation of actin-proficient cellular protrusions. In line with these findings, IRSp53 and LIN7 colocalise at the tips of actin-filled protrusions, whereas IRSp53 is uniformly distributed along those actin-deficient. Notably, LIN7 localisation at the tips depends also on the L27 domain, that not only mediates LIN7 membrane association, but is also necessary and sufficient to direct to the tips the otherwise uniformly distributed IRSp53Δ5 (chimera L27-IRSp53Δ5). Finally, LIN7 lacking the L27 domain, but maintaining the PDZ domain sequesters IRSp53 in the cytoplasm, thus preventing the formation of actin-deficient protrusions. Conversely,

LIN7ΔL27 is not able to retain IRSp53Δ5 in the cytoplasm and to inhibit the formation of actin-deficient protrusions. The essential role for LIN7 association with IRSp53 is further supported by functional interference studies (using RNAi-based downregulation of LIN7C) and structure-function rescue experiments, which collectively argue that the association between LIN7 and IRSp53 is necessary for neuritogenesis. Again, both the L27 and PDZ domains of LIN7 are required to rescue neuritogenesis in N2A cells silenced for LIN7C, the major isoform in these cells, as demonstrated by transient and stable downregulation experiments. These data further suggest that LIN7, through recruitment of IRSp53 to plasma membrane complexes, is a critical early molecular determinant in the formation of these protrusions.

Collectively our data strengthens the crucial importance of LIN7 for IRSp53 function, while arguing against a role exerted by LIN7 in filopodia generated by pathways involving the mDia1 and mDia2 formins. Recently, mDia1, but not mDia2, was shown to be an important SH3 domain partner of IRSp53 in forming filopodia (Goh et al., 2011b). In line with the emerging notion that there are multiple mechanisms regulating the formation of these structures, it is therefore possible that IRSp53 may participate in filopodia formation either through LIN7 or through mDia1, depending on cell context and different stimuli.

Our data, showing that the L27 domain of LIN7 is necessary and sufficient to localise IRSp53 to protrusion tips in NSC34 cells and to promote filopodia and neurite in N2A cells, suggest that interactors of the L27 domains play a crucial role in IRSp53 membrane recruitment. IRSp53 may exist in an autoinhibited state in the cytoplasm, and IRSp53 dimers may become active on the plasma membrane through binding to activated Rho-GTPases (Krugmann et al., 2001). The surface recruitment of IRSp53 is therefore a first crucial step in filopodia extension from the cell periphery, and the L27 domain of LIN7 may accomplish this function.

The L27 domains form heterodimers to achieve their biological functions and to correctly assemble protein complexes and prevent promiscuous binding (Feng et al., 2004; Funke et al., 2005; Shin et al., 2006). Partners of the L27 domain of LIN7 are MAGUK proteins, and multimerisation of these proteins via their L27 domains may be required to link Rho family small GTPases with IRSp53, thus stabilising IRSp53 in its active dimeric form, with its I-BAR and SH3 domains respectively competent for membrane curvature and concentration, at the tips of emergent protrusions, of downstream effectors involved in initiation and bundling of actin filaments. For instance, LIN7 may recruit IRSp53 in the PAR3/PAR6/atypical PKC (protein kinase C) complex that through the guanine nucleotide exchange factor Tiam1 (T-lymphoma invasion and metastasis) control cell-cell junction assembly in epithelia and neurons (Shin et al., 2006), neurite elongation and axon or dendrite fate (Yoshimura et al., 2006).

In agreement with a role for LIN7 in increasing the association of IRSp53 to actin filaments, cells silenced for LIN7 fail to differentiate and to increase the amount of IRSp53 found in the detergent insoluble fraction. Moreover, decreased amount of IRSp53 was found in cell lines stably silenced for LIN7, suggesting that LIN7-mediated recruitment in Triton X-100 insoluble complexes may not only activate but also protect IRSp53 from downregulation.

To conclude, our data identify in LIN7 a novel regulator of IRSp53 that is critical to spatially restrict the LIN7-IRSp53 complex to the plasma membrane for filopodia and neurite initiation, and to further promote the stabilisation of these actin–rich structures. Moreover, underlying the key role of the LIN7:IRSp53 association in neuritogenesis, our results suggest that neurodevelopmental disorders, such as human attention-deficit/hyperactivity disorder (ADHD), recently associated with polymorphisms of LIN7 or IRSp53 or altered expression of LIN7 in humans (Lanktree et al., 2008; Ribases et al., 2009; Zucker et al., 2010; Shinawi et al., 2011) may be due to unbalanced alterations in the expression of LIN7 and/or IRSp53 or to mutations that prevent their interaction.

MATERIALS AND METHODS

Constructs

Generation and subcloning of mouse LIN7A, human IRSp53 constructs and chimeras have been previously described (Massari et al., 2009). The GFP-mDia1, GFP-mDia2 and GFP-IRSp53 cDNAs used in this paper have been described elsewhere (Yang et al., 2009). Small hairpin RNA: two pairs of complementary oligonucleotides containing a 19-nt sequence derived from the messenger RNA transcript of murine LIN7C were synthesised by Invitrogen custom primers: 5'-GGGAAGGTTAAATTAGTCG-3' (shRNA1), and 5'-CGGATAATTCCAGGTGGAA-3' (shRNA2). These sequences did not have any significant homology to other genes in the human genome database and shRNA 2 was chosen from the validated MISSION shRNA library (Sigma, St. Louis, MO). The forward and reverse oligos were annealed and cloned into BglII–XhoI restriction sites of the pSUPER.gfp/neo RNAi system (OligoEngine, Inc., Seattle, WA), followed by amplification of the resulting plasmid. The absence of unwanted substitutions was checked by sequencing (PRIMM, Milan, Italy). Similar results were obtained with the two shRNAs, but all the presented experiments were obtained with shRNA 1 because a higher level of downregulation was measured by Western blot analysis (see Fig. S3 in supplementary material). RFP-pLifeAct (Ibidi GmbH, Martinsried, München, GE) was used to visualise filopodial F-actin in live cell imaging experiments, and a GFP construct fused to a membrane localisation sequence (mGFP) was a kind gift of Dr N. Borgese (Ronchi et al., 2008).

Cell culture and transfection

The NSC34 murine motoneuron-neuroblastoma hybrid cell line (Cashman et al., 1992) were grown in DMEM (Sigma) with 5% FBS (Sigma), 1 mM pyruvate, 1 mM glutamine and antibiotics. Murine neuroblastoma Neuro2A (N2A) cells (Klebe and Ruddle, 1969) were grown in DMEM with 10% FBS, 1 mM glutamine and antibiotics. The cell lines were cultured in a 37°C incubator containing 5% CO_2. Transfections: cDNAs and shRNAs were transiently transfected in NSC34 and N2A cell lines using Lipofectamine 2000 (Invitrogen, Carlsbad, CA), following the manufacturers protocol. For cotransfections 1:1 cDNAs ratio were used. The N2A cell lines stably expressing shRNA LIN7C were selected on the basis of growth in the antibiotic G418 (0.5 mg/ml) (Sigma), and the expression of the construct was assessed by fluorescence microscopy and Western blotting.

Antibodies

Commercial primary antibodies were mouse monoclonal anti-myc (Santa Cruz Biotechnology, Santa Cruz, CA), anti-actin (Sigma) and anti-GFP (MBL, Medical and Biological laboratories Co.,

Japan). The polyclonal rabbit anti-LIN7 antiserum was raised against the histidine-LIN7A fusion protein (Massari et al., 2009); anti-Calnexin (Stressgen, San Diego, CA) and anti-TOM20 (Santa Cruz Biotechnology) were commercial polyclonal antibodies raised in rabbit. The polyclonal rabbit anti-IRSp53 was a kind gift from Dr E. Kim (Korea Advanced Institute of Science and Technology) (Choi et al., 2005).

Triton X-100 cytoskeleton extraction

Detergent extraction experiments were carried out as described (Blikstad and Carlsson, 1982). Briefly, cells were treated for 10 min at 0°C using extraction buffer (0.5% Triton X-100, 100 mM NaF, 50 mM KCl, 2 mM $MgCl_2$, 1 mM EGTA, 10 mM KPO_4, pH 7.5, 0.5 M sucrose) supplemented with PMSF (phenylmethylsulfonyl fluoride) and protease cocktail inhibitor (Sigma) to block the partial depolymerisation of actin seen in other buffers. Cells were collected and sedimented by centrifugation at 13,000 g for 20 min. The supernatant (detergent-soluble fraction containing the G-actin fraction) was taken for immunoblotting. Cell matrice pellets containing F-actin fractions were scraped in the same extraction buffer of the supernatant with a rubber policeman, and both fractions were solubilised with the same volume of sodium dodecyl sulfate (SDS) denaturation buffer. Equal volumes of each fraction were probed by immunoblotting on an 11% SDS-PAGE with the indicated antibodies.

Immunoprecipitation and Western blot analysis

N2A cells grown to 90% confluence in 100 mm dishes were harvested in 1.5 ml of ice-cold lysis buffer (25 mM Tris-HCl pH 7.5, 100 mM NaCl, 5 mM EDTA, 0.5% Triton X-100, 1 mM DTT, PMSF and a cocktail of protease inhibitors) for 30 min at 4°C. The lysates were then spun at 14,000 g for 20 min at 4°C. For input samples, 40 µl of the cell lysate were mixed with 2x SDS samples loading buffer and heated at 100°C for 5 min. For affinity precipitation, 700 µl of lysate were incubated with 25 µl bead volume of protein A–sepharose cross linked to anti-LIN7 antibodies or preimmune IgG at 4°C for 2 h. The immunocomplexes, washed and released from the beads by boiling the samples in SDS solubilisation buffer, and 20 µl of the input sample (3% of the total) were loaded onto a 10% SDS–PAGE, and transferred onto nitrocellulose membranes (PerkinElmer Life Science, Waltham, MA). The blots were probed with the indicated primary antibodies, followed by peroxidase conjugated with mouse IgG or anti-rabbit IgG, light chain specific (Jackson ImmunoResearch Laboratories, West Grove, PA, USA) and proteins were visualised by ECL (PerkinElmer Life Science). Signal intensity was quantified by densitometry using NIH ImageJ 1.59 software.

Immunofluorescence

After being grown and transfected as described, the cells were either used for live-cell imaging (see below) or fixed for 20 min in 4% paraformaldehyde and permeabilised with 0.5% Triton X-100. Immunostaining with primary antibodies was followed by incubation with FITC/CY5 anti-rabbit/mouse antibodies (Jackson Immunoresearch). Rhodamine-labelled phalloidin (Cytoskeleton, Denver, CO) was used to detect filamentous actin. The confocal images were acquired using a Bio-Rad MRC-1024 confocal microscope.

Live-cell imaging

For live-cell imaging experiments, N2A cells were cotransfected with GFP tagged IRSp53 constructs (IRSp53 and L27-IRSp53) or with mGFP as a control and RFP-pLifeAct. Twenty-four hours after transfection, cells were serum-starved for additional 16 h and then placed in an environmentally controlled chamber with 5% CO_2 at 37°C, using an Axiovert 200M (Zeiss) confocal system equipped with spinning-disc (PerkinElmer). A 100X objective and the 488/561 nm laser lines were used for acquisition of GFP fusion proteins or RFP-LifeAct, respectively. Images were collected every 20 s for a period of 10 min; thirty still images of each recording session were analysed for the emergence and retraction of protrusions.

The unbranched, dynamic, actin-containing protrusions with a mean length of 3.44 μm ± 0.36 and half-life of 173 s ± 1 were defined filopodia; the branched and unbranched protrusions, poorly stained with phalloidin, unchanging their length and position from time zero to the end of the analysis (5 min), were respectively defined branched and linear static protrusions. For each transfectant a total of at least 400 μm of plasma membrane from 10 different cells obtained in two separate experiments were analysed. Image analysis was performed with the Volocity High-Performance Imaging System (PerkinElmer). To measure lifetime: sixty protrusions from 10 different cells obtained from two separate experiments were recorded. The number of frames from the point of emergence of individual filopodia to its complete loss was determined and multiplied by 20 s to achieve the lifetime. To determine the mean number of filopodia in 100 μm plasma membrane: for each transfectant were analysed a total of at least 400 μm of plasma membrane from 10 different cells obtained in two separate experiments, and the total number of filopodia that protruded or retracted in the selected region of the membrane during the 5 min time-lapse were quantified.

Image and statistical analysis

Morphological phenotypes in NSC34 cells were quantified using the following definitions. Actin-filled protrusions: thin elongated structures (average length between 5-10 μm and width of 0.5-1 μm) positively stained by labelled phalloidin for their entire length. Actin-deficient protrusions: protrusions corresponding to both linear and branched structures emerging from the plasma membrane not stained for their entire length with labelled phalloidin.

Quantification of the signals was evaluated by using ImageJ plot profile. To count cell protrusions, the Adobe Photoshop software filters “trace contour” and “find edges” were sequentially applied at the outlined protrusions above described, and the average total number of actin-filled and actin-deficient protrusions was obtained by manual counting in at least 20 different cells (6 mm of total plasma membrane) for each transfectant.

For neurite quantification, after 48 h serum-starvation, cells were fixed in 4% paraformaldehyde for 20 min at 37°C, and viewed with a Zeiss Axioplan inverted phase contrast microscope (40X objective) connected with an AxioCam HRm CCD camera. Neurites were defined as processes with a length of at least a cell body diameter, and this definition in no way attributes any functional value to these structures and is purely a reflection of morphological similarity to neurites.

A total of 300 cells for each transfectant were examined in randomly chosen fields from three independent experiments. All quantitative data are presented as mean ± s.e.m.; multiple comparisons among groups were carried out by Student’s t test using Prism software (GraphPad PrismTM software).

ACKNOWLEDGEMENTS

We thank Sara Colombo for advices on immunoprecipitation experiments. This work was supported by fellowship from Fondazione Fratelli Confalonieri (to V.P.), grants (to G.S. and A.D) from the Associazione Italiana per la Ricerca sul Cancro (AIRC), grants (to D.F) from CARIPLO (2010-0688). G.S. was also supported by the Italian Ministries of Education-University-Research (MIUR-PRIN) and of Health, the CARIPLO Foundations and the European Research Council (Advanced ERC-2010).

REFERENCES

Ahmed, S., Goh, W. I. and Bu, W. (2010). I-BAR domains, IRSp53 and filopodium formation. *Semin Cell Dev Biol* **21**, 350-356.

Barilari, M. and Dente, L. (2010). The neuronal proteins CIPP, Cypin and IRSp53 form a tripartite complex mediated by PDZ and SH3 domains. *Biol Chem* **391**, 1169-1174.

Blikstad, I. and Carlsson, L. (1982). On the dynamics of the microfilament system in HeLa cells. *J Cell Biol* **93**, 122-128.

Block, J., Stradal, T. E., Hanisch, J., Geffers, R., Kostler, S. A., Urban, E., Small, J. V., Rottner, K. and Faix, J. (2008). Filopodia formation induced by active mDia2/Drf3. *J Microsc* **231**, 506-517.

Cashman, N. R., Durham, H. D., Blusztajn, J. K., Oda, K., Tabira, T., Shaw, I. T., Dahrouge, S. and Antel, J. P. (1992). Neuroblastoma x spinal cord (NSC) hybrid cell lines resemble developing motor neurons. *Dev Dyn* **194**, 209-221.

Chetkovich, D. M., Chen, L., Stocker, T. J., Nicoll, R. A. and Bredt, D. S. (2002). Phosphorylation of the postsynaptic density-95 (PSD-95)/discs large/zona occludens-1 binding site of stargazin regulates binding to PSD-95 and synaptic targeting of AMPA receptors. *J Neurosci* **22**, 5791-5796.

Choi, J., Ko, J., Racz, B., Burette, A., Lee, J. R., Kim, S., Na, M., Lee, H. W., Kim, K., Weinberg, R. J. et al. (2005). Regulation of dendritic spine morphogenesis by insulin receptor substrate 53, a downstream effector of Rac1 and Cdc42 small GTPases. *J Neurosci* **25**, 869-879.

Cohen, D., Fernandez, D., Lazaro-Dieguez, F. and Musch, A. (2011). The serine/threonine kinase Par1b regulates epithelial lumen polarity via IRSp53-mediated cell-ECM signaling. *J Cell Biol* **192**, 525-540.

Dent, E. W., Kwiatkowski, A. V., Mebane, L. M., Philippar, U., Barzik, M., Rubinson, D. A., Gupton, S., Van Veen, J. E., Furman, C., Zhang, J. et al. (2007). Filopodia are required for cortical neurite initiation. *Nat Cell Biol* **9**, 1347-1359.

Faix, J. and Rottner, K. (2006). The making of filopodia. *Curr Opin Cell Biol* **18**, 18-25.

Faix, J. and Grosse, R. (2006). Staying in shape with formins. *Dev Cell* **10**, 693-706.

Feng, W., Long, J. F., Fan, J. S., Suetake, T. and Zhang, M. (2004). The tetrameric L27 domain complex as an organization platform for supramolecular assemblies. *Nat Struct Mol Biol* **11**, 475-480.

Funke, L., Dakoji, S. and Bredt, D. S. (2005). Membrane-associated guanylate kinases regulate adhesion and plasticity at cell junctions. *Annu Rev Biochem* **74**, 219-245.

Gilbert, M. and Fulton, A. B. (1985). The specificity and stability of the triton-extracted cytoskeletal framework of gerbil fibroma cells. *J Cell Sci* **73**, 335-345.

Goh, W. I., Sudhaharan, T., Lim, K. B., Sem, K. P., Lau, C. L. and Ahmed, S. (2011a). Rif-mDia1 interaction is involved in filopodium formation independent of Cdc42 and Rac effectors. *J Biol Chem* **286**, 13681-13694.

Goh, W. I., Lim, K. B., Sudhaharan, T., Sem, K. P., Bu, W., Chou, A. M. and Ahmed, S. (2011b). mDia1 and WAVE2 interact directly with IRSp53 in filopodia and are involved in filopodium formation. *J Biol Chem* **287**, 4702-4714.

Hori, K., Konno, D., Maruoka, H. and Sobue, K. (2003). MALS is a binding partner of IRSp53 at cell-cell contacts. *FEBS Lett* **554**, 30-34.

Jo, K., Derin, R., Li, M. and Bredt, D. S. (1999). Characterization of MALS/Velis-1, -2, and -3: a family of mammalian LIN-7 homologs enriched at brain synapses in association with the postsynaptic density-95/NMDA receptor postsynaptic complex. *J Neurosci* **19**, 4189-4199.

Klebe, R. J. and Ruddle, F. H. (1969). Neuroblastoma:Cell culture analysis of a differentiating stem cell system. *J. Cell. Biol* **43**, 69H.

Krugmann, S., Jordens, I., Gevaert, K., Driessens, M., Vandekerckhove, J. and Hall, A. (2001). Cdc42 induces filopodia by promoting the formation of an IRSp53:Mena complex. *Curr Biol* **11**, 1645-1655.

Lanktree, M., Squassina, A., Krinsky, M., Strauss, J., Jain, U., Macciardi, F., Kennedy, J. L. and Muglia, P. (2008). Association study of brain-derived neurotrophic factor (BDNF) and LIN-7 homolog (LIN-7) genes with adult attention-deficit/hyperactivity disorder. *Am J Med Genet B Neuropsychiatr Genet* **147B**, 945-951.
Lee, Y. G., Macoska, J. A., Korenchuk, S. and Pienta, K. J. (2002). MIM, a potential metastasis suppressor gene in bladder cancer. *Neoplasia* **4**, 291-294.
Lowery, L. A. and Van Vactor, D. (2009). The trip of the tip: understanding the growth cone machinery. *Nat Rev Mol Cell Biol* **10**, 332-343.
Massari, S., Perego, C., Padovano, V., D'Amico, A., Raimondi, A., Francolini, M. and Pietrini, G. (2009). LIN7 mediates the recruitment of IRSp53 to tight junctions. *Traffic* **10**, 246-257.
Mattila, P. K., Pykalainen, A., Saarikangas, J., Paavilainen, V. O., Vihinen, H., Jokitalo, E. and Lappalainen, P. (2007). Missing-in-metastasis and IRSp53 deform PI(4,5)P2-rich membranes by an inverse BAR domain-like mechanism. *J Cell Biol* **176**, 953-964.
Miki, H. and Takenawa, T. (2002). WAVE2 serves a functional partner of IRSp53 by regulating its interaction with Rac. *Biochem Biophys Res Commun* **293**, 93-99.
Miyahara, A., Okamura-Oho, Y., Miyashita, T., Hoshika, A. and Yamada, M. (2003). Genomic structure and alternative splicing of the insulin receptor tyrosine kinase substrate of 53-kDa protein. *J Hum Genet* **48**, 410-414.
Nakagawa, H., Miki, H., Nozumi, M., Takenawa, T., Miyamoto, S., Wehland, J. and Small, J. V. (2003). IRSp53 is colocalised with WAVE2 at the tips of protruding lamellipodia and filopodia independently of Mena. *J Cell Sci* **116**, 2577-2583.
Okamura-Oho, Y., Miyashita, T. and Yamada, M. (2001). Distinctive tissue distribution and phosphorylation of IRSp53 isoforms. *Biochem Biophys Res Commun* **289**, 957-960.
Olsen, O., Moore, K. A., Fukata, M., Kazuta, T., Trinidad, J. C., Kauer, F. W., Streuli, M., Misawa, H., Burlingame, A. L., Nicoll, R. A. et al. (2005). Neurotransmitter release regulated by a MALS-liprin-alpha presynaptic complex. *J Cell Biol* **170**, 1127-1134.
Olsen, O., Funke, L., Long, J. F., Fukata, M., Kazuta, T., Trinidad, J. C., Moore, K. A., Misawa, H., Welling, P. A., Burlingame, A. L. et al. (2007). Renal defects associated with improper polarization of the CRB and DLG polarity complexes in MALS-3 knockout mice. *J Cell Biol* **179**, 151-164.
Perego, C., Vanoni, C., Massari, S., Longhi, R. and Pietrini, G. (2000). Mammalian LIN-7 PDZ proteins associate with beta-catenin at the cell-cell junctions of epithelia and neurons. *Embo J* **19**, 3978-3989.
Ribases, M., Bosch, R., Hervas, A., Ramos-Quiroga, J. A., Sanchez-Mora, C., Bielsa, A., Gastaminza, X., Guijarro-Domingo, S., Nogueira, M., Gomez-Barros, N. et al. (2009). Case-control study of six genes asymmetrically expressed in the two cerebral hemispheres: association of BAIAP2 with attention-deficit/hyperactivity disorder. *Biol Psychiatry* **66**, 926-934.
Ronchi, P., Colombo, S., Francolini, M. and Borgese, N. (2008). Transmembrane domain-dependent partitioning of membrane proteins within the endoplasmic reticulum. *J Cell Biol* **181**, 105-118.
Scita, G., Confalonieri, S., Lappalainen, P. and Suetsugu, S. (2008). IRSp53: crossing the road of membrane and actin dynamics in the formation of membrane protrusions. *Trends Cell Biol* **18**, 52-60.
Shin, K., Fogg, V. C. and Margolis, B. (2006). Tight junctions and cell polarity. *Annu Rev Cell Dev Biol* **22**, 207-235.
Shinawi, M., Sahoo, T., Maranda, B., Skinner, S. A., Skinner, C., Chinault, C., Zascavage, R., Peters, S. U., Patel, A., Stevenson, R. E. et al. (2011). 11p14.1 microdeletions associated with ADHD, autism, developmental delay, and obesity. *Am J Med Genet A* **155**, 1272-1280.
Wu, G., Fang, Y., Lu, Z. H. and Ledeen, R. W. (1998). Induction of axon-like and dendrite-like processes in neuroblastoma cells. *J Neurocytol* **27**, 1-14.

Yang, C. and Svitkina, T. (2011). Filopodia initiation: focus on the Arp2/3 complex and formins. *Cell Adh Migr* **5**, 402-408.
Yang, C., Hoelzle, M., Disanza, A., Scita, G. and Svitkina, T. (2009). Coordination of membrane and actin cytoskeleton dynamics during filopodia protrusion. *PLoS One* **4**, e5678.
Yang, C., Czech, L., Gerboth, S., Kojima, S., Scita, G. and Svitkina, T. (2007). Novel roles of formin mDia2 in lamellipodia and filopodia formation in motile cells. *PLoS Biol* **5**, e317.
Yoshimura, T., Arimura, N. and Kaibuchi, K. (2006). Signaling networks in neuronal polarization. *J Neurosci* **26**, 10626-10630.
Zhao, H., Pykalainen, A. and Lappalainen, P. (2011). I-BAR domain proteins: linking actin and plasma membrane dynamics. *Curr Opin Cell Biol* **23**, 14-21.
Zheng, C. Y., Seabold, G. K., Horak, M. and Petralia, R. S. (2011). MAGUKs, Synaptic Development, and Synaptic Plasticity. *Neuroscientist* **17**, 493-512.
Ziv, N. E. and Smith, S. J. (1996). Evidence for a role of dendritic filopodia in synaptogenesis and spine formation. *Neuron* **17**, 91-102.
Zucker, B., Kama, J. A., Kuhn, A., Thu, D., Orlando, L. R., Dunah, A. W., Gokce, O., Taylor, D. M., Lambeck, J., Friedrich, B. et al. (2010). Decreased Lin7b expression in layer 5 pyramidal neurons may contribute to impaired corticostriatal connectivity in huntington disease. *J Neuropathol Exp Neurol* **69**, 880-895.

FIGURE LEGENDS

Fig. 1. Colocalisation of IRSp53 and LIN7 to protrusion tips depends on the L27 domain of LIN7 and the PDZ target motif of IRSp53. A) Schematic representation of the domain organisation of LIN7 and IRSp53 constructs used in the study. The myc or GFP tags fused at the N-termini and the domain structures are indicated; deleted domains are indicated with the X. (**B-C**) NSC34 cells were transiently transfected with the indicated cDNAs (left). Three days after transfection, cells were fixed in paraformaldehyde and stained with the myc antibody to localise IRSp53 and rhodamine-conjugated phalloidin to localise F-actin; localisation of LIN7 constructs is revealed by the GFP fluorescence. Merged images and individual staining of the selected magnified protrusions are shown. The signal quantifications were obtained using ImageJ "plot profile". Pixel intensity along the corresponding protrusions is expressed in fluorescence arbitrary units (a.u.); tip and base of filopodia are indicated. Bars: 5 μm. **(D).** A summary of localisation analysis, such as those in panels B and C, shows the examined constructs and their presence or absence in protrusions and protrusion tips.

Fig. 2. LIN7 regulates the protrusion-promoting activity of IRSp53. NSC34 cells transfected with the indicated cDNAs were analysed by immunocytochemistry **(A-D)** or Western blot **(E)**. **(**A-C) Cells were fixed in paraformaldehyde 3 days after transfection with the indicated cDNAs (top of each image), stained with rhodamine-conjugated phalloidin to localise F-actin and anti-myc antibody to localise IRSp53 constructs; LIN7 constructs were revealed by the GFP fluorescence. GFP-tagged empty vector was transfected as control (CTR). Merged images of the indicated double staining, and inset magnification (individual staining) of linear and branched protrusions boxed in the myc-IRSp53 and IRSp53Δ5 merged images. The histograms represent the percentage of actin-deficient protrusions (linear + branched) measured in 20 different cells (6 mm of total plasma membrane) for each transfectant. Bars: 10 μm. (D) Quantification of total protrusion average (actin-deficient + actin-filled) in 100 μm of plasma membrane obtained by measuring the protrusions in N>20 cells. Data are the means of at least three independent experiments. Error bars indicates ± s.e.m.; p values (t-test) are indicated. (E) Detergent extraction experiment. Equal volumes of insoluble F- and soluble G-actin fractions were loaded in 11% SDS-PAGE and blotted onto nitrocellulose; the amount of actin in each fraction was evaluated using specific antibodies. The molecular weight (kDa) is indicated on the right of the blot. Quantification showing mean ± s.e.m. of three independent experiments (one of which is shown) is presented as percentage of F- and G-actin; p value (t-test) is indicated.

Fig. 3. L27-IRSp53 induces dynamic protrusions in differentiated N2A. (**A-C**) Cells were cotransfected with RFP-LifeAct and membrane mGFP construct as control (A), GFP- IRSp53 (B) or GFP-L27-IRSp53 (C). Twenty-four h after transfection the cells were serum starved for additional 16 h. Whole cells are shown in the merged images (left), magnifications of the selected areas at the indicated time points are presented separately (green and red channels) and merged. Bars: 5 μm. Filopodia were measured for lifetime **(D)**, percentage of static linear protrusions showing absence of assembly/disassembly **(E)**, and average number of filopodia in 100 μm membrane (**F**). The graph (**G)** represents the changes in length of filopodia during the 5 min analysis and the unchanged length of 4 branched actin-deficient protrusions in cells expressing IRSp53. Quantification showing mean ± s.e.m. of two independent experiments; p values (t-test) are indicated.

Fig. 4. IRSp53 requires LIN7 to induce neurite outgrowth in undifferentiated N2A cells. **(A)** Western blot characterisation of the expression of LIN7 and IRSp53 isoforms in N2A cells by immunoprecipitation with anti-LIN7 antibodies (IP: LIN7) or preimmune IgG (IP: preimmune serum). The presence of IRSp53 isoforms in the immunocomplexes was determined by immunoprobing the nitrocellulose membranes with anti-IRSp53 antibodies (IB: IRSp53), and immunoprecipitation of LIN7 was verified by using anti-LIN7 antibodies (IB: LIN7). Three per cent of cell lysate was probed with the same antibodies (Input). Bands 1, 2 with the relative molecular mass corresponding to de-phosphorylated and phosphorylated IRSp53-S; band 3 of the apparent molecular mass of the IRSp53-L; bands 4 and 5 with the apparent molecular mass of IRSp53-S dimers and tetramers, respectively. The arrow indicates the IgG light chain dimers recognised by peroxidase conjugated antibody. **(B)** A representative Western blot showing downregulation of LIN7C in N2A cells transiently transfected with shRNA 1. Ten micrograms of total protein extracts from control and silenced N2A cells were probed with a pan-LIN7 antibody for the expression of LIN7 isoforms, and with corresponding specific antibodies to probe IRSp53 and Calnexin, the latter used as a loading control. The molecular weights (kDa) are indicated on the right of the blot. The histogram representing the percentage of LIN7 in silenced cells compared to control was obtained by densitometric quantification of the 22 kDa band (corresponding to LIN7B and/or C) normalised to Calnexin. Data are the means ± s.e.m. of four independent experiments; p value (t-test) compared to control is indicated. **(C)** Laser confocal microscopy of undifferentiated N2A cells transfected with the empty vector (pSUPER), the cDNA encoding GFP-IRSp53 (IRSp53) or cotransfected with GFP-IRSp53 and shRNA LIN7C cDNAs. Merged images show GFP-positive transfected cells, and phalloidin staining for actin in red. The insets show magnifications (2,2X) of

the process outlined in the merged image. Bar: 20 μm. **(D)** Undifferentiated N2A cells transfected with the cDNA encoding formin mDia2 or cotransfected with mDia2 and shRNA LIN7C cDNAs were analysed by laser confocal microscopy. Merged images show GFP-positive signal transfected cells, and phalloidin staining for actin in red. Bar: 20 μm. **(E)** Quantification of the percentage of cells with neurites (N>150 cells). Data are the means of three independent experiments. Error bars indicate ± s.e.m.; p values (t-test) are indicated.

Fig. 5. IRSp53 requires LIN7 association for neurite outgrowth. (A) Phase contrast comparison of differentiated N2A cells transfected with the pSUPER empty vector (CTR), the vector encoding shRNA LIN7C or cotransfected with shRNA LIN7C and the indicated constructs. Transfected cells are identified by the green signal. Twenty-four hours after transfection, cells were serum-starved for additional 48 h to induce neurite outgrowth before fixation in 4% paraformaldehyde. Bar: 40 μm. **(B)** The histogram represents the effects of the transfectants on differentiated N2A cells; neurite outgrowth was scored by evaluating the percentage of cells with neurites. Data are the means ± s.e.m. of three independent experiments; processes in N>100 cells for each experiment were evaluated. P values (t-test) compared to control are indicated.

Fig. 6. LIN7 increases Triton X-100 detergent insolubility of IRSp53 in differentiated N2A cells. (A) Western blot analysis of the amount of IRSp53 and LIN7 in Triton X-100 insoluble (I) and soluble (S) fractions. Undifferentiated N2A cells cultured in medium with 10% FBS (CTR+FBS) or differentiated in medium without serum (CTR-FBS) for 48 h were extracted in 0.5% Triton X-100 for 10 min at 0°C. Equivalent volumes of Triton X-100-insoluble or -soluble fractions were separated by 11% SDS-PAGE and immunostained for the indicated markers. The corresponding molecular weights (kDa) are indicated on the right of the blots. Representative immunoblots and densitometric quantification (expressed as % of the total I+S immunoreactivity) of two independent experiments are presented. The histogram on the right represents the values obtained by measuring the percentage of immunoreactivity in the insoluble fractions compared to that of CTR+FBS (CTR+FBS =1). Data are the means ± s.e.m. and p values (t-test) compared to control are indicated. **(B)** Western blot analysis of the level of expression of LIN7 and IRSp53 in the selected (2, 5 and 9) N2A clones specifically knocked down for LIN7C protein expression by shRNA 1. Ten micrograms of total protein extracts from control N2A cells (CTR) and N2A cells stably expressing shRNA were probed for LIN7 and IRSp53 expression; Calnexin was probed as a loading control. The corresponding molecular weights (kDa) are indicated on the right. **(C)** Confocal laser analysis of shRNA LIN7C clone 9 in undifferentiated (+FBS) or differentiated (-

FBS) culture conditions. The expression of shRNA LIN7C (green) and staining of F-actin (red) are shown. Bar: 15 µm. **(D)** Western blot analysis of the amount of IRSp53 in Triton X-100 insoluble (I) and soluble (S) fractions from undifferentiated (+FBS) or differentiated (-FBS) N2A cells stably silenced for LIN7C. A representative immunoblot and the densitometric quantification (expressed as % of the total I+S immunoreactivity) of two independent experiments performed with clone 9 are shown. The histogram on the right represents the values ± s.e.m. of two independent experiments each one performed in both clones 2 and 9. Data were obtained by measuring the percentage of immunoreactivity in the insoluble fractions of clones 2 and 9 (2+9) compared to the percentage of immunoreactivity in the insoluble fraction of CTR+FBS (CTR+FBS =1).

SUPPLEMENTARY MATERIAL

Fig. S1. Levels of expression of IRSp53 (full length or mutants) in NSC34 cells transiently cotransfected with LIN7 or the pSUPER plasmid. A representative Western blot analysis is shown. Total protein extracts were probed (IB:) for IRSp53 and TOM20, the latter used as a loading control. Molecular weight standards are indicated on the left. The histogram representing the IRSp53 level of expression in the indicated cotransfection normalised to cotransfection with control pSUPER plasmid was obtained by densitometric quantification of IRSp53 bands normalised to TOM20.

Fig. S2. Levels of expression of IRSp53 or L27-IRSp53 in N2A cells transiently transfected with the corresponding GFP-tagged cDNAs. A representative Western blot is shown. Total protein extracts were probed for IRSp53 and TOM20, the latter used as a loading control. Molecular weight standards are indicated on the left. The histogram representing the level of expression of the chimera L27-IRSp53 compared to IRSp53 was obtained by densitometric quantification of IRSp53 bands normalised to TOM20.

Fig. S3. Laser confocal microscopy of differentiated N2A cells transiently transfected with shRNAs for LIN7C (shRNA 1 and shRNA 2). Transfected cells were identified by the green signal, while the red signal identifies the phalloidin staining for F-actin. Merged images are shown. Bar: 20 μm The histogram representing the level of expression of LIN7 and IRSp53 in silenced cells compared to control cells (CTR) was obtained by densitometric quantification of IRSp53 and LIN7 bands normalised to Calnexin. Data are the means ± s.e.m. of two independent experiments; p values (t-test) compared to control are indicated.

Fig. S4. Western blot analysis of the level of expression of the indicated IRSp53 or LIN7 constructs transiently co-transfected with shRNA LIN7C in N2A cells. Total protein extracts were probed (IB:) for GFP or IRSp53 and for TOM20, as a loading control. Molecular weight standards are indicated on the left. The histograms represent the level of expression of LIN7ΔPDZ compared to LIN7 or L27-IRSp53 compared to IRSp53 in cells cotransfected with shRNA 1, and were obtained by densitometric quantification of GFP or IRSp53 bands normalised to TOM20.

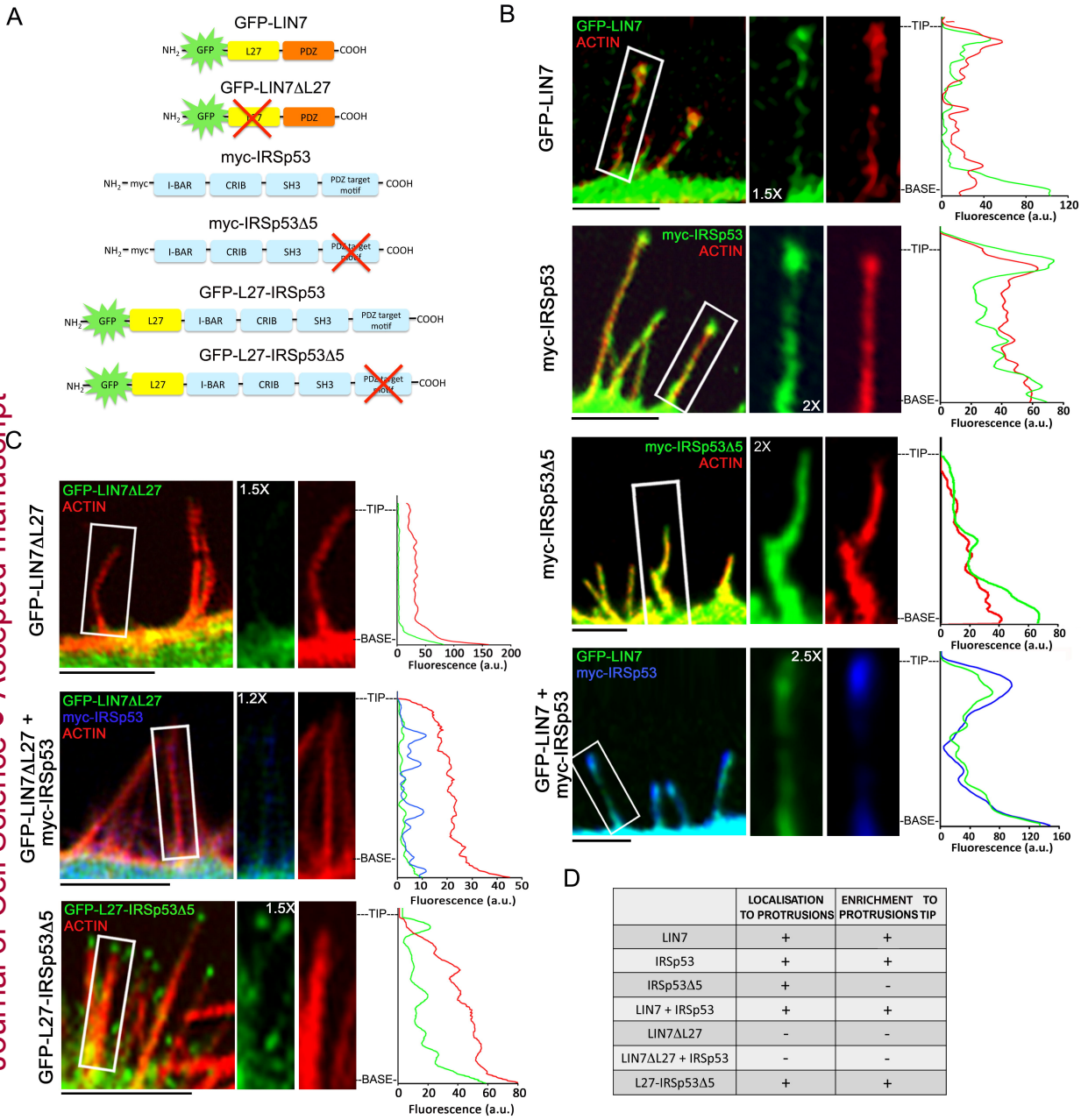

D

	LOCALISATION TO PROTRUSIONS	ENRICHMENT TO PROTRUSIONS TIP
LIN7	+	+
IRSp53	+	+
IRSp53Δ5	+	-
LIN7 + IRSp53	+	+
LIN7ΔL27	-	-
LIN7ΔL27 + IRSp53	-	-
L27-IRSp53Δ5	+	+

Figure 1

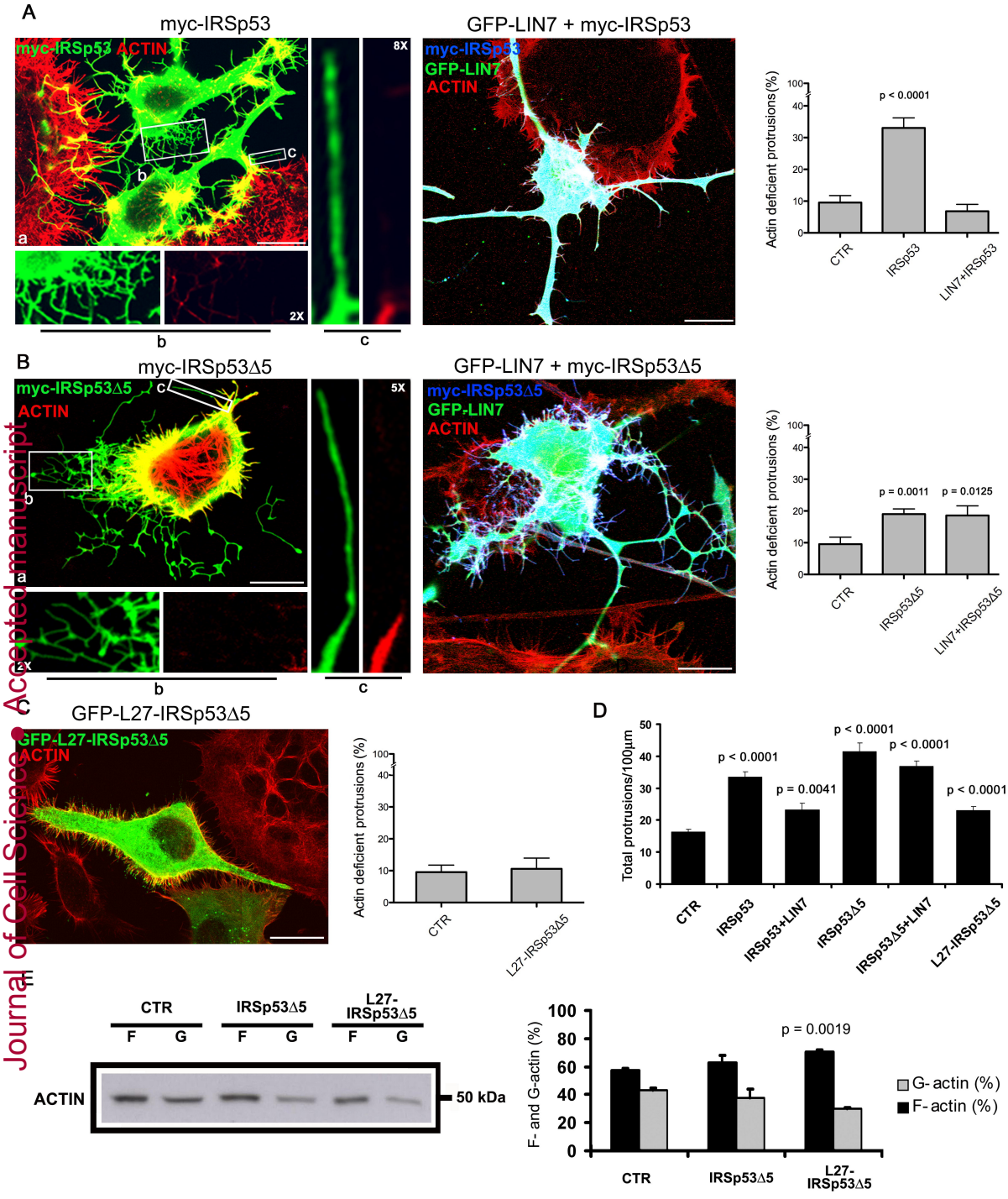

Figure 2

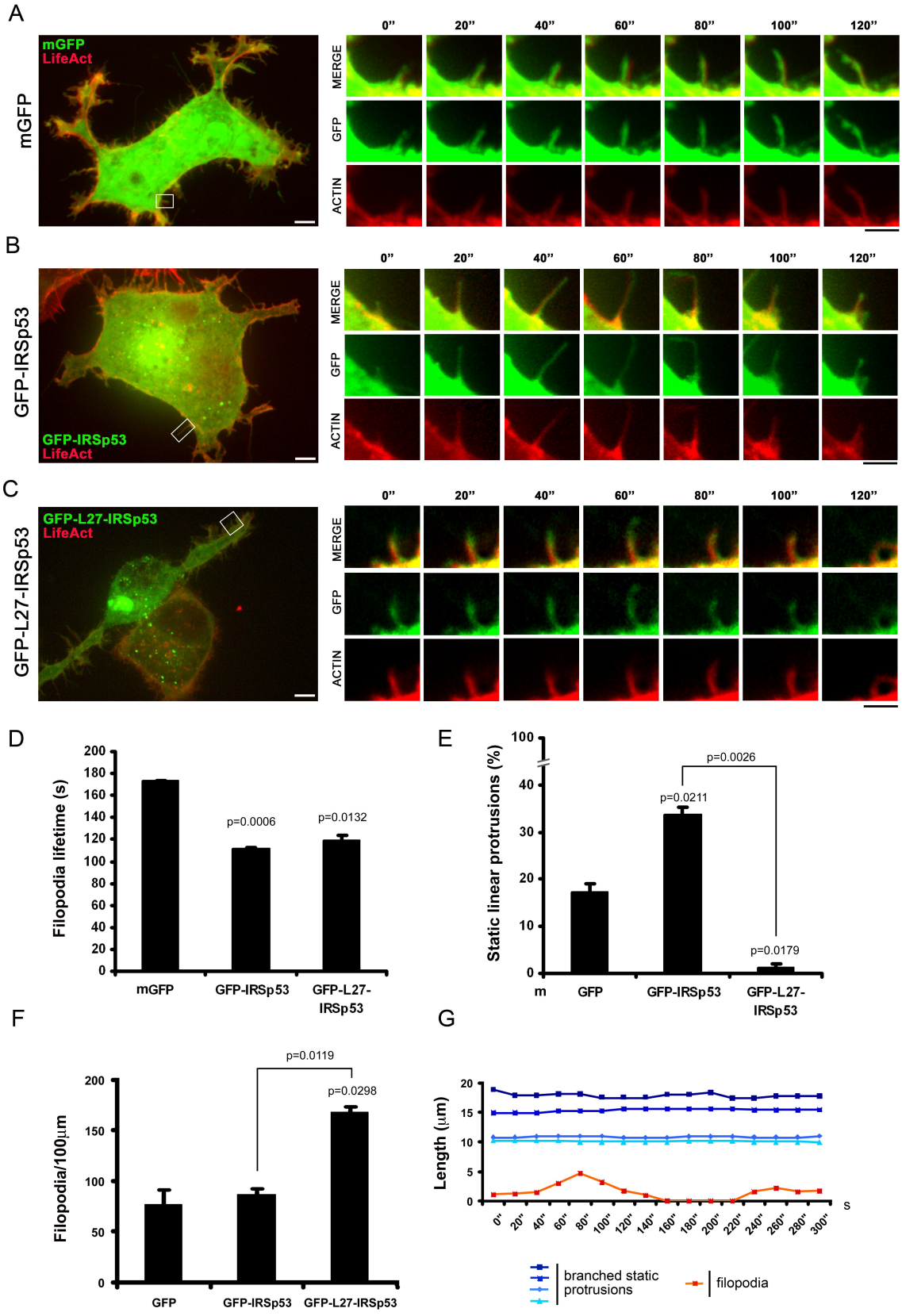

Figure 3

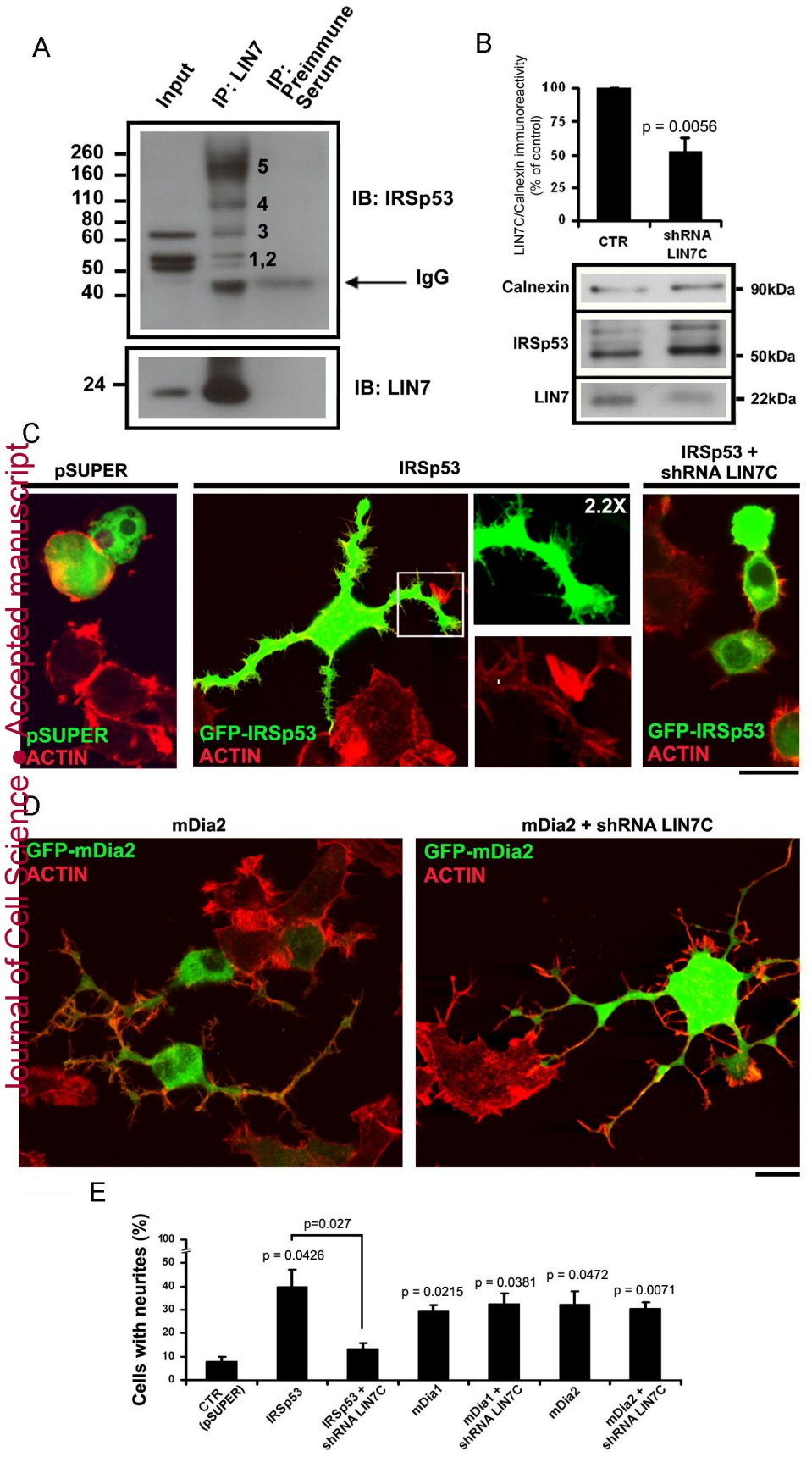

Figure 4

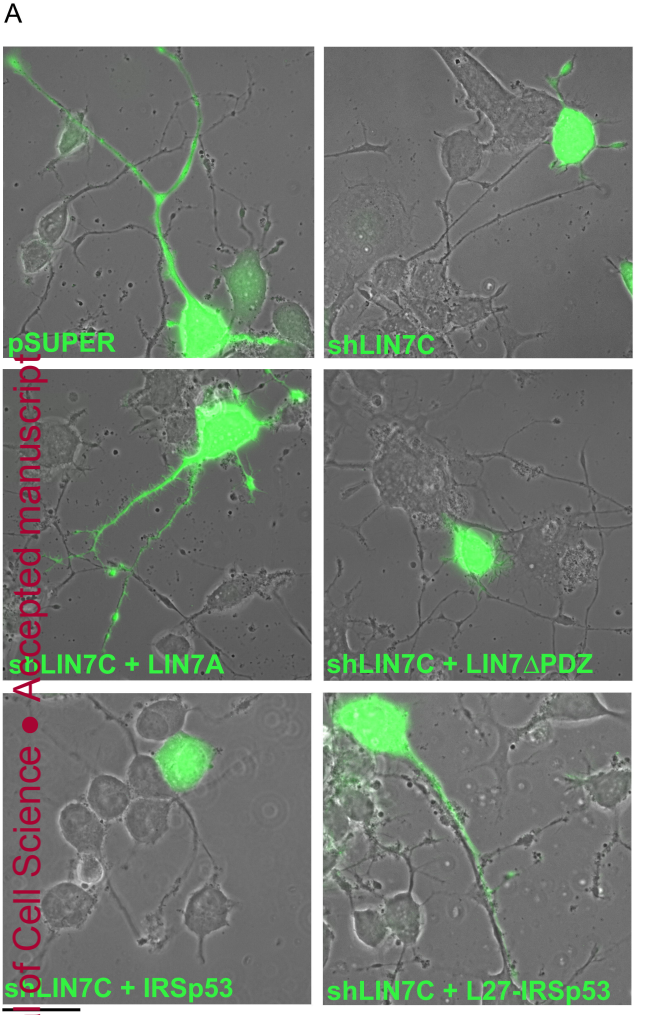

Figure 5

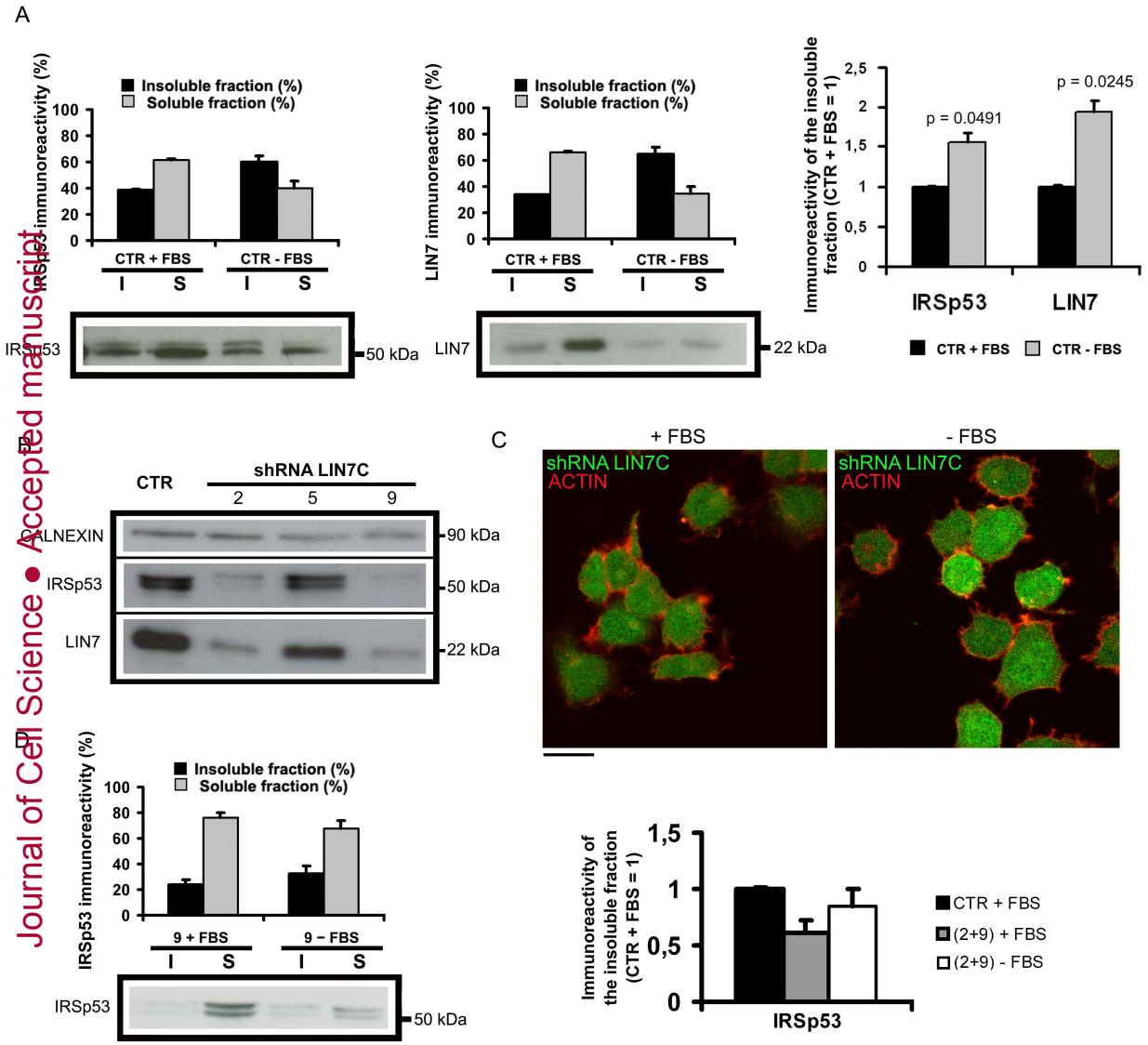

Figure 6